Chapter 5
UAV Relay Communications

Xinyu Zheng, Jiliang Zhang, and Gaofeng Pan

5.1 On Secrecy Analysis of Underlay Cognitive UAV-Aided NOMA Systems with Transmit Antenna Selection/Maximal-Ratio Combining (TAS/MRC)

This section investigates the secrecy performance of a UAV-aided NOMA network in the context of underlay CR. Specifically, a multi-antenna secondary source (S) transmits a mixed signal incorporated with NOMA to two multi-antenna secondary destinations (D_i) via a UAV-enabled DF relay in the presence of an eavesdropper (E). In addition, both a transmit antenna selection scheme at S and a maximal ratio combining protocol at D_i and E are considered. Considering all the links undergo Nakagami-m fading with path loss, we analyze the secrecy performance in terms of SOP for both users. Moreover, we also use Monte Carlo simulations to verify those expressions.

The main contributions are as follows:

(1) We study the secrecy performance for an underlay CR UAV-aided NOMA system. The scenario of a TAS scheme at a secondary source, the MRC protocol at the destinations, and the parallel PIC at the eavesdropper are considered.
(2) The PDF and CDF of all links are first characterized when all the links experience both large-scale and small-scale fading. Then, utilizing those expressions, we derive both users' closed-form expressions of the SOP.
(3) We also investigate the impact of several parameters, i.e., the number of antennas, power distribution coefficient, the height of the UAV, and interference power threshold, on the secrecy performance.

X. Zheng · J. Zhang
Southwest University, Chongqing, China
e-mail: swuzhang@swu.edu.cn

G. Pan (✉)
Beijing Institute of Technology, Beijing, China
e-mail: gfpan@bit.edu.cn

G. Pan et al. (eds.), *UAV Communications: Modeling and Analyses*,
https://doi.org/10.1007/978-981-97-0383-8_5

(4) Finally, we analyze the effect of the hovering position of the UAV and the flight trajectory on the secrecy performance.

5.2 System and Channel Models

As shown in Fig. 5.1, an underlay CR UAV-aided NOMA system is considered in this analysis, which includes a L_S-antenna secondary source (S), a single antenna UAV-relay (R), two multi-antenna secondary destinations, i.e., a L_{D_1}-antenna far user (D_1) and a L_{D_2}-antenna near user (D_2), and a L_E-antenna eavesdropper (E). Note that the UAV is a relay in this system to link the information transmission from S to destinations.

Unlike the traditional ground relaying system, due to the advantage of mobility, it is easier and faster to deploy the UAV-enabled relaying system, especially in natural disasters. Furthermore, the LoS link is more likely to be established with the UAV-enabled relay [1, 2]. It is assumed that there is no direct link between S and both two users due to deep fading and/or obstacle blocking.

We also assume that E can only overhear the second hop, and this assumption is reasonable. In a practical scenario, it may be difficult for E to find a suitable position to wiretap both hops as the UAV is allocated in a proper deployment position to build reliable links to serve both users well. Therefore, from the eavesdropping point of view and to guarantee that it can overhear the information of both users, E may adopt a strategy to locate itself on the destination side. The symbol, $d_{Rg} = \sqrt{K_{Rg}^2 + H^2}$, is used to indicate the distance between nodes R and g, where $g \in \{S,\ D_i,\ E\}$, and H and K_{Rg} denote the vertical distance of node R to the ground and the horizontal

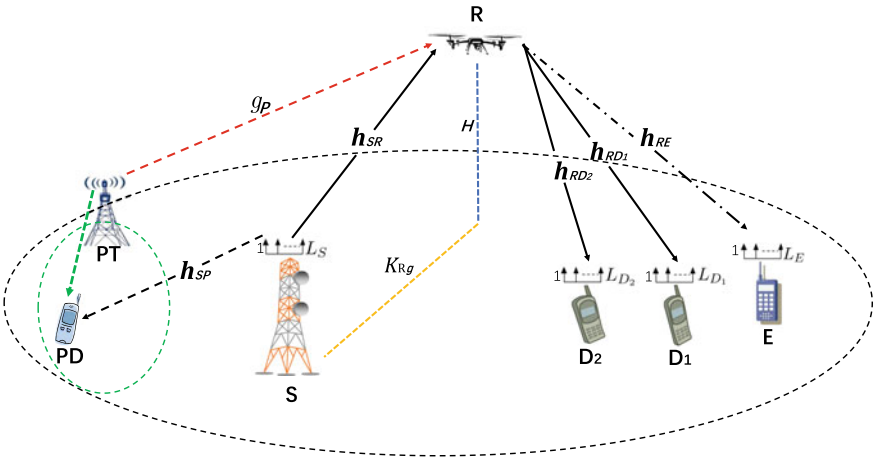

Fig. 5.1 System model

distance to node g, respectively. It is noted that the measured results from [3, 4] showed that in the suburban/open filed environment, the performance of the UAV communication system is significantly affected by path loss.

Moreover, according to the experimental results, the UAV channels in low-altitude applications can be more appropriately modeled as Nakagami-m distributions [5]. Therefore, all links are assumed to undergo Nakagami-m fading with a path loss, and h_{ab} ($a, b \in \{P,\ S,\ R,\ D_i,\ E\}$) is used to denote the channel coefficient between nodes a and b with a fading parameter m_{ab} and an average channel power gain $\Omega_{ab} = E\{|h_{ab}|^2\}$. Therefore, the channel power gains, $|h_{ab}|^2$, follows a gamma distribution with the PDF and CDF expressed as

$$f_{|h_{ab}|^2}(x) = \frac{\beta_{ab}^{m_{ab}} x^{m_{ab}-1}}{\Gamma(m_{ab})} \exp(-\beta_{ab} x) \tag{5.1}$$

and

$$F_{|h_{ab}|^2}(x) = 1 - \sum_{i=0}^{m_{ab}-1} \frac{\beta_{ab}^i x^i}{i!} \exp(-\beta_{ab} x), \tag{5.2}$$

where $\beta_{ab} = \frac{m_{ab}}{\Omega_{ab}}$ and $\Gamma(\cdot)$ is defined as gamma function shown by [6, Eq. (8.339.1)].

In the first time slot, S adopts the selected antenna after performing the TAS scheme to transmit a mixed signal $x_{SR} = \sum_{i=1}^{2} \sqrt{\alpha_i P_s} x_i$ to R under the underlay cognitive radio model, where α_i means the power allocation factor satisfying $\alpha_1 + \alpha_2 = 1$ and $\alpha_1 > \alpha_2$, and x_i means the signal of D_i with $\mathrm{E}|x_i|^2 = 1$. The transmit power of S is denoted as $P_s = \frac{I_{th}}{|h_{SP}|^2}$, where I_{th} is the interference threshold at the primary destination.

Similar to [7, 8], the interference signal from the primary transmitter is modeled as AWGN to simplify the theoretical analysis. Thus, the signal received by R is denoted as

$$y_{SR} = \frac{h_{SR}^{\max}}{\sqrt{d_{SR}^{\theta}}} x_{SR} + n_R + g_P, \tag{5.3}$$

where n_R is the zero mean AWGN with a variance of N_R, and g_P is the interference signal from PT, which is with $\mathcal{CN}(0, \eta N_R)$, and η is the scaling coefficient of g_P, $|h_{SR}^{\max}| = \max_{1 \le l_S \le L_S} \left| h_{SR}^{l_S} \right|$, with $h_{SR}^{l_S}$ means the channel coefficient between l_S-th antenna of S and R, and θ is the path loss exponent.

Similar to [9, 10], perfect SIC is employed in this analysis. Therefore, the far user's signal, x_1, is first decoded at R, and then x_1 is removed from the mixed signal before decoding x_2. Hence, it has the SNR and SINR for D_2 and D_1 at R as

$$\gamma_{SR}^{D_2} = \frac{\alpha_2 \rho_{SR} |h_{SR}^{\max}|^2}{(\eta + 1) d_{SR}^{\theta}} \tag{5.4}$$

and

$$\gamma_{SR}^{D_1} = \frac{\alpha_1 \rho_{SR} |h_{SR}^{\max}|^2}{\alpha_2 \rho_{SR} |h_{SR}^{max}|^2 + (\eta + 1) d_{SR}^{\theta}}, \tag{5.5}$$

respectively, where $\rho_{SR} = \frac{P_s}{N_R}$.

Next, the CDF of $|h_{SR}^{max}|^2$ can be obtained as

$$F_{|h_{SR}^{max}|^2}(x) = \left[1 - \sum_{i=0}^{m_{SR}-1} \frac{\beta_{SR}^i x^i}{i!} \exp(-\beta_{SR} x) \right]^{L_S}. \tag{5.6}$$

In the second time slot, the DF protocol, which eliminates the influence of the first hop on the second hop in the dual-hop communication, is adopted at R to process the received signal. Therefore, R first decodes the received signal and then forwards the re-encoded one to D_i in the presence of E. Hence, the received signals at l_{D_i}-th antenna of D_i and at l_E-th antenna of E can be written as

$$y_{RD_i}^{l_{D_i}} = \frac{h_{RD_i}^{l_{D_i}}}{\sqrt{d_{RD_i}^{\theta}}} x_{RD} + n_{D_i} \tag{5.7}$$

and

$$y_{RE}^{l_E} = \frac{h_{RE}^{l_E}}{\sqrt{d_{RE}^{\theta}}} x_{RD} + n_E, \tag{5.8}$$

respectively, where n_{D_i} and n_E are the zero mean AWGN with variances of N_{D_i} and N_E at D_i and E, and $x_{RD} = \sum_{i=1}^{2} \sqrt{\alpha_i P_R} x_i$, and P_R is the transmit power at R. Moreover, $h_{RD_i}^{l_{D_i}}$ and $h_{RE}^{l_E}$ denote the channel coefficients for the l_{D_i}-th antenna of the D_i and l_E-th antenna of E, respectively.

Next, D_i adopts the MRC scheme to process the received signals. Meanwhile, SIC is also performed. Specifically, the far user D_1 decodes its signal while treating D_2's signal as interference. While the near user, D_2, first decodes and subtracts D_1's signal and then processes its signal.

Therefore, it has the instantaneous SINR at D_1 and the SNR at D_2 as

$$\gamma_{RD_1} = \frac{\rho_{RD_1} \alpha_1 |h_{RD_1}|^2}{\alpha_2 \rho_{RD_1} |h_{RD_1}|^2 + d_{RD_1}^{\theta}} \tag{5.9}$$

and

$$\gamma_{RD_2} = \frac{\rho_{RD_2}\alpha_2|h_{RD_2}|^2}{d_{RD_2}^{\theta}}, \tag{5.10}$$

respectively, where $\rho_{RD_i} = \frac{P_R}{N_{D_i}}$ and $|h_{RD_i}|^2 = \sum_{l_{D_i}=1}^{L_{D_i}} |h_{RD_i}^{l_{D_i}}|^2$.

Making use of Eqs. (5.2), (5.9), and (5.10), the CDFs of γ_{RD_1} and γ_{RD_2} can be obtained as

$$F_{\gamma_{RD_1}}(x) = \begin{cases} 1 - \sum_{i=0}^{m_{RD_1}L_{D_1}-1} \frac{(d_{RD_1}^{\theta}\beta_{RD_1})^i x^i}{[\rho_{RD_1}(\alpha_1-\alpha_2 x)]^i i!} \exp\left(-\frac{\beta_{RD_1} d_{RD_1}^{\theta} x}{\rho_{RD_1}(\alpha_1-\alpha_2 x)}\right), & \text{if } x < \frac{\alpha_1}{\alpha_2}; \\ 1, & \text{else} \end{cases} \tag{5.11}$$

and

$$F_{\gamma_{RD_2}}(x) = 1 - \sum_{j=0}^{m_{RD_2}L_{D_2}-1} \frac{(\beta_{RD_2} d_{RD_2}^{\theta})^j x^j}{(\alpha_2\rho_{RD_2})^j j!} \exp\left(-\frac{\beta_{RD_2} d_{RD_2}^{\theta} x}{\alpha_2\rho_{RD_2}}\right), \tag{5.12}$$

respectively.

In addition, we conduct this analysis under the assumption that E has the largest decoding ability. Specifically, the MRC technique is applied at E to process the received signal. The PIC is also employed to decode the superimposed signals, i.e., the interference from x_1 (x_2) can be eliminated when decoding x_2 (x_1). Hence, the SNRs for the signals of D_1 and D_2 at E can be expressed as

$$\gamma_{RE}^{D_1} = \frac{\alpha_1\rho_{RE}|h_{RE}|^2}{d_{RE}^{\theta}} = \alpha_1\gamma_{RE} \tag{5.13}$$

and

$$\gamma_{RE}^{D_2} = \frac{\alpha_2\rho_{RE}|h_{RE}|^2}{d_{RE}^{\theta}} = \alpha_2\gamma_{RE}, \tag{5.14}$$

where $\rho_{RE} = \frac{P_R}{N_E}$, $|h_{RE}|^2 = \sum_{l_E=1}^{L_E} |h_{RE}^{l_E}|^2$, and $\gamma_{RE} = \frac{\rho_{RE}|h_{RE}|^2}{d_{RE}^{\theta}}$ with the PDF of γ_{RE} denoted as

$$f_{\gamma_{RE}}(x) = \frac{(\beta_{RE} d_{RE}^{\theta})^{m_{RE}L_E} x^{m_{RE}L_E-1}}{\rho_{RE}{}^{m_{RE}L_E}\Gamma(m_{RE}L_E)} \exp\left(-\frac{\beta_{RE} d_{RE}^{\theta} x}{\rho_{RE}}\right). \tag{5.15}$$

5.3 Secrecy Performance Analysis

In this section, the derivation of SOPs for two users is presented.

5.3.1 SOP Analysis

5.3.1.1 SOP of D_1

The instantaneous SC of D_1 for the two links can be expressed as

$$C_{SR}^{D_1} = \frac{1}{2}\log_2\left(1+\gamma_{SR}^{D_1}\right) \tag{5.16}$$

and

$$C_{RD_1} = \left\{\frac{1}{2}\log_2\frac{1+\gamma_{RD_1}}{1+\gamma_{RE}^{D_1}}\right\}^+, \tag{5.17}$$

where$\{x\}^+ = \max\{x, 0\}$.

The worst hop in the DF relaying system dominates the system capacity. Hence, the SC of D_1 as

$$C_{D_1} = \min\left\{C_{SR}^{D_1}, C_{RD_1}\right\}. \tag{5.18}$$

A secrecy outage occurs when the instantaneous SC exceeds the user's threshold requirement, C_{th_1}. Therefore, it has the SOP of D_1 as

$$\begin{aligned}
P_{SOP}^{D_1} &= \Pr\left\{C_{D_1} < C_{th_1}\right\} \\
&= \Pr\left\{\min\left\{C_{SR}^{D_1}, C_{RD_1}\right\} < C_{th_1}\right\} \\
&= 1 - \Pr\left\{C_{SR}^{D_1} \geq C_{th_1}, C_{RD_1} \geq C_{th_1}\right\} \\
&= 1 - \Pr\left\{C_{SR}^{D_1} \geq C_{th_1}\right\}\Pr\left\{C_{RD_1} \geq C_{th_1}\right\} \\
&= 1 - \Pr\left\{\gamma_{SR}^{D_1} \geq C_{T_1} - 1\right\}\Pr\left\{\gamma_{RD_1} \geq C_{T_1}(1+\gamma_{RE}^{D_1}) - 1\right\},
\end{aligned} \tag{5.19}$$

where $C_{T_1} = 2^{2C_{th_1}}$.

Based on Eqs. (5.1), (5.5), and (5.6), we have

$$\begin{aligned}\Pr\left\{\gamma_{SR}^{D_1} \geq C_{T_1} - 1\right\} &= \Pr\left\{|h_{SR}^{\max}|^2 \geq \gamma_{th_1}|h_{SP}|^2\right\} \\ &= \int_0^\infty \left[1 - F_{|h_{SR}^{\max}|^2}(\gamma_{th_1}x)\right] f_{|h_{SP}|^2}(x)dx \\ &= 1 - \int_0^\infty \frac{\beta_{SP}^{m_{SP}} x^{m_{SP}-1}}{\Gamma(m_{SP})} \exp(-\beta_{SP}x) \\ &\quad \times \underbrace{\left[1 - \exp(-\beta_{SR}\gamma_{th_1}x) \sum_{i=0}^{m_{SR}-1} \frac{(\beta_{SR}\gamma_{th_1}x)^i}{i!}\right]^{L_S}}_{J} dx,\end{aligned} \tag{5.20}$$

where $\gamma_{th_1} = \frac{(C_{T_1}-1)(\eta+1)d_{SR}^{\theta}}{\rho_I(\alpha_1-\alpha_2(C_{T_1}-1))}$ and $\rho_I = \frac{I_{th}}{N_R}$.

Applying the binomial theorem to the term, J, in Eq. (5.20), it has

$$\begin{aligned}J &= \sum_{k=0}^{L_S} \binom{L_S}{k} (-1)^k \exp(-k\beta_{SR}\gamma_{th_1}x) \left[\sum_{i=0}^{m_{SR}-1} \frac{(\beta_{SR}\gamma_{th_1}x)^i}{i!}\right]^k \\ &= \sum_{k=0}^{L_S} \binom{L_S}{k} (-1)^k \exp(-k\beta_{SR}\gamma_{th_1}x) \prod_{i=0}^{m_{SR}-2} \left(\frac{(\beta_{SR}\gamma_{th_1})^i}{i!}\right)^{k_{i+1}} \\ &\quad \times \sum_{k_1=0}^{k} \sum_{k_2=0}^{k-k_1} \cdots \sum_{k_{m_{SR}-1}=0}^{k-k_1-\cdots-k_{m_{SR}-2}} \binom{k}{k_1}\binom{k-k_1}{k_2}\cdots\binom{k-k_1-\cdots-k_{m_{SR}-2}}{k_{m_{SR}}-1} \\ &\quad \times \left(\frac{(\beta_{SR}\gamma_{th_1})^{m_{SR}-1}}{(m_{SR}-1)!}\right)^{k-k_1-\cdots-k_{m_{SR}-1}} x^{\Theta},\end{aligned} \tag{5.21}$$

where $\Theta = (m_{SR}-1)(k-k_1) - (m_{SR}-2)k_2 - \cdots - 2k_{m_{SR}-2} - k_{m_{SR}-1}$.

Defining

$$\Phi = \sum_{k_1=0}^{k} \sum_{k_2=0}^{k-k_1} \cdots \sum_{k_{m_{SR}-1}=0}^{k-k_1-\cdots-k_{m_{SR}-2}} \binom{k}{k_1}\binom{k-k_1}{k_2}\cdots\binom{k-k_1-\cdots-k_{m_{SR}-2}}{k_{m_{SR}}-1}, \tag{5.22}$$

$$\Psi_1 = \left(\frac{(\beta_{SR}\gamma_{th_1})^{m_{SR}-1}}{(m_{SR}-1)!}\right)^{k-k_1-\cdots-k_{m_{SR}-1}} \prod_{i=0}^{m_{SR}-2} \left(\frac{(\beta_{SR}\gamma_{th_1})^i}{i!}\right)^{k_{i+1}}, \tag{5.23}$$

and substituting Eq. (5.21) into Eq. (5.20), we have

$$\begin{aligned}\Pr\left\{\gamma_{SR}^{D_1} \geq C_{T_1} - 1\right\} &= 1 - \int_0^{\infty} \sum_{k=0}^{L_S} \binom{L_S}{k} (-1)^k \exp(-k\beta_{SR}\gamma_{th_1} x) \Phi \Psi_1 x^{\Theta} \\ &\quad \times \frac{\beta_{SP}^{m_{SP}} x^{m_{SP}-1}}{\Gamma(m_{SP})} \exp(-\beta_{SP} x) dx \\ &= 1 - \sum_{k=0}^{L_S} \binom{L_S}{k} (-1)^k \Phi \Psi_1 \frac{\beta_{SP}^{m_{SP}}}{\Gamma(m_{SP})} \\ &\quad \times \int_0^{\infty} x^{\Theta + m_{SP} - 1} \exp\left[-(k\beta_{SR}\gamma_{th_1} + \beta_{SP}) x\right] dx \\ &= 1 - \sum_{k=0}^{L_S} \binom{L_S}{k} (-1)^k \Phi \Psi_1 \frac{\beta_{SP}^{m_{SP}}}{\Gamma(m_{SP})} (\Theta + m_{SP} - 1)! \\ &\quad \times (k\beta_{SR}\gamma_{th_1} + \beta_{SP})^{-\Theta - m_{SP}}. \end{aligned} \tag{5.24}$$

Based on Eqs. (5.11), and (5.15), it has

$$\begin{aligned}\Pr\left\{\gamma_{RD_1} \geq C_{T_1}(1 + \gamma_{RE}^{D_1}) - 1\right\} &= 1 - \left[\int_0^t F_{\gamma_{RD_1}}(C_{T_1}(1 + \alpha_1 x) - 1) f_{\gamma_{RE}}(x) dx \right. \\ &\quad \left. + \int_t^{\infty} f_{\gamma_{RE}}(x) dx\right] \\ &= \int_0^t \left[1 - F_{\gamma_{RD_1}}(C_{T_1}(1 + \alpha_1 x) - 1)\right] f_{\gamma_{RE}}(x)\, dx \\ &= \int_0^t \exp\left[-\frac{\beta_{RD_1} d_{RD_1}^{\theta} (C_{T_1} - 1 + C_{T_1}\alpha_1 x)}{\rho_{RD_1}(\alpha_1 - \alpha_2(C_{T_1} - 1 + C_{T_1}\alpha_1 x))}\right] \\ &\quad \cdot \sum_{j=0}^{m_{RD_1} L_{D_1} - 1} \frac{\beta_{RD_1}^j (d_{RD_1}^{\theta})^j (C_{T_1} - 1 + C_{T_1}\alpha_1 x)^j}{j!(\rho_{RD_1}(\alpha_1 - \alpha_2(C_{T_1} - 1 + C_{T_1}\alpha_1 x)))^j} \\ &\quad \cdot \frac{(\beta_{RE} d_{RE}^{\theta})^{m_{RE} L_E} x^{m_{RE} L_E - 1}}{\rho_{RE}^{m_{RE} L_E} \Gamma(m_{RE} L_E)} \exp\left(-\frac{\beta_{RE} d_{RE}^{\theta} x}{\rho_{RE}}\right) dx, \end{aligned} \tag{5.25}$$

where $t = \frac{\frac{\alpha_1}{\alpha_2} + 1 - C_{T_1}}{\alpha_1 C_{T_1}}$.

Since the closed-form expression for Eq. (5.25) is difficult to obtain, the Gaussian Chebyshev quadrature [6] is applied to obtain an approximated expression as

$$\Pr\left\{\gamma_{RD_1} \geq C_{T_1}(1+\gamma_{RE}^{D_1})-1\right\} = \frac{(\beta_{RE} d_{RE}^{\theta})^{\mu_{RE}}}{\rho_{RE}^{\mu_{RE}}\Gamma(\mu_{RE})} \sum_{j=0}^{\mu_{RD_1}-1} \frac{(\beta_{RD_1} d_{RD_1}^{\theta})^{j}}{j!} \frac{t}{2}\frac{\pi}{N}$$
$$\cdot \sum_{n=1}^{N} \frac{(C_{T_1}-1+C_{T_1}\alpha_1\tau)^{j}}{\left[\rho_{RD_1}(\alpha_1-\alpha_2(C_{T_1}+C_{T_1}\alpha_1\tau-1))\right]^{j}}$$
$$\cdot \exp\left[\frac{(1-C_{T_1}-C_{T_1}\alpha_1\tau)\beta_{RD_1} d_{RD_1}^{\theta}}{\rho_{RD_1}(\alpha_1-\alpha_2(C_{T_1}+C_{T_1}\alpha_1\tau-1))}\right]$$
$$\cdot \exp\left(-\frac{\beta_{RE} d_{RE}^{\theta}}{\rho_{RE}}\tau\right)\tau^{\mu_{RE}-1}\sqrt{1-\phi^2}, \tag{5.26}$$

where N is a factor of the Gaussian-Chebyshev term, and $\phi = \cos(\frac{2n-1}{2N}\pi)$, $\tau = \frac{t}{2}(\phi+1)$, $\mu_{RD_i} = m_{RD_i} L_{D_i}$, $\mu_{RE} = m_{RE} L_E$.

Applying Eqs. (5.21), and (5.25), we express the analytical expression of SOP for D_1 as

$$P_{SOP}^{D_1} = 1 - \left[1 - \sum_{k=0}^{L_S}\binom{L_S}{k}(-1)^k \Phi\Psi_1 \frac{\beta_{SP}^{m_{SP}}}{\Gamma(m_{SP})}(\Theta+m_{SP}-1)!\right.$$
$$\left.\times (k\beta_{SR}\gamma_{th_1}+\beta_{SP})^{-\Theta-m_{SP}}\right] \frac{(\beta_{RE} d_{RE}^{\theta})^{\mu_{RE}}}{\rho_{RE}^{\mu_{RE}}\Gamma(\mu_{RE})} \sum_{j=0}^{\mu_{RD_1}-1} \frac{(\beta_{RD_1} d_{RD_1}^{\theta})^{j}}{j!}$$
$$\times \frac{t}{2}\frac{\pi}{N}\sum_{n=1}^{N} \frac{(C_{T_1}-1+C_{T_1}\alpha_1\tau)^{j}}{\left[\rho_{RD_1}(\alpha_1-\alpha_2(C_{T_1}+C_{T_1}\alpha_1\tau-1))\right]^{j}}$$
$$\times \exp\left[\frac{(1-C_{T_1}-C_{T_1}\alpha_1\tau)\beta_{RD_1} d_{RD_1}^{\theta}}{\rho_{RD_1}(\alpha_1-\alpha_2(C_{T_1}+C_{T_1}\alpha_1\tau-1))}\right]$$
$$\times \exp\left(-\frac{\beta_{RE} d_{RE}^{\theta}}{\rho_{RE}}\tau\right)\tau^{\mu_{RE}-1}\sqrt{1-\phi^2}. \tag{5.27}$$

5.3.1.2 SOP of D_2

The instantaneous SC for D_2 is

$$C_{D_2} = \min\left\{C_{SR}^{D_2}, C_{RD_2}\right\}, \tag{5.28}$$

where

$$C_{SR}^{D_2} = \frac{1}{2}\log_2\left(1+\gamma_{SR}^{D_2}\right) \tag{5.29}$$

and

$$C_{RD_2} = \left\{ \frac{1}{2}\log_2 \frac{\left(1+\gamma_{RD_2}\right)}{\left(1+\gamma_{RE}^{D_2}\right)} \right\}^+. \tag{5.30}$$

Next, the SOP of D_2 is expressed as

$$\begin{aligned} P_{SOP}^{D_2} &= \Pr\left\{C_{D_2} < C_{th_2}\right\} \\ &= \Pr\left\{\min(C_{SR}^{D_2}, C_{RD_2}) < C_{th_2}\right\} \\ &= 1 - \Pr\left\{C_{SR}^{D_2} \geq C_{th_2}, C_{RD_2} \geq C_{th_2}\right\} \\ &= 1 - \Pr\left\{C_{SR}^{D_2} \geq C_{th_2}\right\} \Pr\left\{C_{RD_2} \geq C_{th_2}\right\} \\ &= 1 - \Pr\left\{\gamma_{SR}^{D_2} \geq C_{T_2} - 1\right\} \Pr\left\{\gamma_{RD_2} \geq C_{T_2}(1+\gamma_{RE}^{D_2}) - 1\right\}, \end{aligned} \tag{5.31}$$

where $C_{T_2} = 2^{2C_{th_2}}$ and C_{th_2} is the capacity threshold of D_2.

From Eqs. (5.1), (5.4), and (5.6), we have

$$\begin{aligned} \Pr\left\{\gamma_{SR}^{D_2} \geq C_{T_2} - 1\right\} &= \Pr\left\{|h_{SR}^{max}|^2 \geq \gamma_{th_2}|h_{SP}|^2\right\} \\ &= \int_0^\infty \left[1 - F_{|h_{SR}^{max}|^2}(\gamma_{th_2} x)\right] f_{|h_{SP}|^2}(x) dx \\ &= 1 - \sum_{k=0}^{L_S} \binom{L_S}{k} (-1)^k \Phi \Psi_2 \frac{\beta_{SP}^{m_{SP}}}{\Gamma(m_{SP})} (\Theta + m_{SP} - 1)! \\ &\quad \times (k\beta_{SR}\gamma_{th_2} + \beta_{SP})^{-\Theta - m_{SP}}, \end{aligned} \tag{5.32}$$

where $\Psi_2 = \prod_{i=0}^{m_{SR}-2} \left(\frac{(\beta_{SR}\gamma_{th_2})^i}{i!}\right)^{k_{i+1}} \left(\frac{(\beta_{SR}\gamma_{th_2})^{m_{SR}-1}}{(m_{SR}-1)!}\right)^{k-k_1-\cdots-k_{m_{SR}-1}}$ and $\gamma_{th_2} = \frac{(C_{T_2}-1)(\eta+1)d_{SR}^{\theta}}{\rho_I \alpha_2}$.

After that, from Eqs. (5.12) and (5.15), and (3.326.2) in [6], it has

$$\begin{aligned}\Pr\left\{\gamma_{RD_2} \geq C_{T_2}(1+\gamma_{RE}^{D_2})-1\right\} &= \int_0^{\infty}\left[1-F_{\gamma_{RD_2}}(C_{T_2}(1+\alpha_2 x)-1)\right] f_{\gamma_{RE}}(x)\,dx \\ &= \int_0^{\infty}\sum_{j=0}^{\mu_{RD_2}-1}\frac{(\beta_{RD_2}d_{RD_2}^{\theta})^j (C_{T_2}-1+C_{T_2}\alpha_2 x)^j}{(\alpha_2\rho_{RD_2})^j\, j!} \\ &\quad \cdot \exp\left(-\frac{\beta_{RD_2}d_{RD_2}^{\theta}(C_{T_2}-1+C_{T_2}\alpha_2 x)}{\alpha_2\rho_{RD_2}}\right) \\ &\quad \cdot \frac{\beta_{RE}^{\mu_{RE}}(d_{RE}^{\theta})^{\mu_{RE}} x^{\mu_{RE}-1}}{\rho_{RE}^{\mu_{RE}}\Gamma(\mu_{RE})}\exp\left(-\frac{\beta_{RE}d_{RE}^{\theta}x}{\rho_{RE}}\right)dx \\ &= \frac{(\beta_{RE}d_{RE}^{\theta})^{\mu_{RE}}}{\rho_{RE}^{\mu_{RE}}\Gamma(\mu_{RE})}\exp\left(-\frac{\beta_{RD_2}d_{RD_2}^{\theta}(C_{T_2}-1)}{\alpha_2\rho_{RD_2}}\right) \\ &\quad \cdot \sum_{j=0}^{\mu_{RD_2}-1}\frac{(\beta_{RD_2}d_{RD_2}^{\theta})^j}{(\alpha_2\rho_{RD_2})^j\, j!}\sum_{q=0}^{j}\binom{j}{q}(C_{T_2}-1)^{j-q} \\ &\quad \times (C_{T_2}\alpha_2)^q \frac{\Gamma(\mu_{RE}+q)}{\left(\beta_{RD_2}d_{RD_2}^{\theta}\frac{C_{T_2}}{\rho_{RD_2}}+\frac{\beta_{RE}d_{RE}^{\theta}}{\rho_{RE}}\right)^{\mu_{RE}+q}}.\end{aligned} \tag{5.33}$$

Finally, from Eqs. (5.31) and (5.32), the SOP of D_2 can be derived as

$$\begin{aligned}P_{SOP}^{D_2} &= 1-\left(1-\sum_{k=0}^{L_S}\binom{L_S}{k}(-1)^k \Phi\Psi_2 \frac{\beta_{SP}^{m_{SP}}}{\Gamma(m_{SP})}(\Theta+m_{SP}-1)!\right. \\ &\quad \left.\times (k\beta_{SR}\gamma_{th_2}+\beta_{SP})^{-\Theta-m_{SP}}\right)\frac{(\beta_{RE}d_{RE}^{\theta})^{\mu_{RE}}}{\rho_{RE}^{\mu_{RE}}\Gamma(\mu_{RE})} \\ &\quad \times \exp\left(-\frac{\beta_{RD_2}d_{RD_2}^{\theta}(C_{T_2}-1)}{\alpha_2\rho_{RD_2}}\right)\sum_{j=0}^{\mu_{RD_2}-1}\frac{(\beta_{RD_2}d_{RD_2}^{\theta})^j}{(\alpha_2\rho_{RD_2})^j\, j!}\sum_{q=0}^{j}\binom{j}{q} \\ &\quad \times (C_{T_2}-1)^{j-q}(C_{T_2}\alpha_2)^q \frac{\Gamma(\mu_{RE}+q)}{\left(\beta_{RD_2}d_{RD_2}^{\theta}\frac{C_{T_2}}{\rho_{RD_2}}+\frac{\beta_{RE}d_{RE}^{\theta}}{\rho_{RE}}\right)^{\mu_{RE}+q}}.\end{aligned} \tag{5.34}$$

5.3.2 *Asymptotic Analysis*

To enhance the study, a theoretical insight in terms of asymptotic analysis for both users is provided in this section to show the significance of the analytical results in the high SNR regimes, revealing the system's performance limits.

For D_1, let $\rho_I \to \infty$ (i.e.,$\gamma_{th_1} \to 0$), while ρ_{RD_1} keeps fixed and finite, it has $\lim_{\gamma_{th_1}\to 0} \exp(-k\beta_{SR}\gamma_{th_1}x) = 1$. Therefore, the asymptotic expression can be obtained as

$$
\begin{aligned}
P_{SOP_1}^{\rho_I\to\infty} = 1-\Big(1-\sum_{k=0}^{L_S}\binom{L_S}{k}(-1)^k\beta_{SP}^{m_{SP}}(k\beta_{SR}\gamma_{th_1}+\beta_{SP})^{-m_{SP}}\Big) \\
\times \frac{(\beta_{RE}d_{RE}^{\theta})^{\mu_{RE}}}{\rho_{RE}^{\mu_{RE}}\Gamma(\mu_{RE})}\sum_{j=0}^{\mu_{RD_1}-1}\frac{(\beta_{RD_1}d_{RD_1}^{\theta})^j}{j!}\frac{t}{2}\frac{\pi}{N} \\
\times \sum_{n=1}^{N}\frac{(C_{T_1}-1+C_{T_1}\alpha_1\tau)^j}{\big[\rho_{RD_1}(\alpha_1-\alpha_2(C_{T_1}+C_{T_1}\alpha_1\tau-1))\big]^j} \\
\times \exp\left[\frac{(1-C_{T_1}-C_{T_1}\alpha_1\tau)\beta_{RD_1}d_{RD_1}^{\theta}}{\rho_{RD_1}(\alpha_1-\alpha_2(C_{T_1}+C_{T_1}\alpha_1\tau-1))}\right] \\
\times \exp\left(-\frac{\beta_{RE}d_{RE}^{\theta}}{\rho_{RE}}\tau\right)\tau^{\mu_{RE}-1}\sqrt{1-\phi^2}. \qquad (5.35)
\end{aligned}
$$

Next, let $\rho_{RD_1} \to \infty$ while ρ_I keeps fixed and finite. Making use of the first two terms of the Taylor series expansion, the asymptotic expression of D_1 can be obtained as

$$
\begin{aligned}
P_{SOP_1}^{\rho_{RD_1}\to\infty} = 1-\Big(1-\sum_{k=0}^{L_S}\binom{L_S}{k}(-1)^k\Phi\Psi_1\frac{\beta_{SP}^{m_{SP}}}{\Gamma(m_{SP})} \\
\times (\Theta+m_{SP}-1)!(k\beta_{SR}\gamma_{th_1}+\beta_{SP})^{-\Theta-m_{SP}}\Big) \\
\times \frac{(\beta_{RE}d_{RE}^{\theta})^{\mu_{RE}}}{\rho_{RE}^{\mu_{RE}}\Gamma(\mu_{RE})}\sum_{j=0}^{\mu_{RD_1}-1}\frac{(\beta_{RD_1}d_{RD_1}^{\theta})^j}{j!}\frac{t}{2}\frac{\pi}{N} \\
\times \sum_{n=1}^{N}\frac{(C_{T_1}-1+C_{T_1}\alpha_1\tau)^j}{\big[\rho_{RD_1}(\alpha_1-\alpha_2(C_{T_1}+C_{T_1}\alpha_1\tau-1))\big]^j} \\
\times \left[1+\frac{(1-C_{T_1}-C_{T_1}\alpha_1\tau)\beta_{RD_1}d_{RD_1}^{\theta}}{\rho_{RD_1}(\alpha_1-\alpha_2(C_{T_1}+C_{T_1}\alpha_1\tau-1))}\right] \\
\times \exp\left(-\frac{\beta_{RE}d_{RE}^{\theta}}{\rho_{RE}}\tau\right)\tau^{\mu_{RE}-1}\sqrt{1-\phi^2}. \qquad (5.36)
\end{aligned}
$$

Applying the approaches, we can respectively obtain the asymptotic expressions when $\rho_I \to \infty$ and $\rho_{RD_2} \to \infty$ for D_2 as

$$
\begin{aligned}
P_{SOP_2}^{\rho_I \to \infty} = 1 - \Big(1 - \sum_{k=0}^{L_S} \binom{L_S}{k} (-1)^k \beta_{SP}^{m_{SP}} \\
\times (k\beta_{SR}\gamma_{th_2} + \beta_{SP})^{-m_{SP}}\Big) \\
\times \frac{(\beta_{RE} d_{RE}^{\theta})^{\mu_{RE}}}{\rho_{RE}^{\mu_{RE}} \Gamma(\mu_{RE})} \exp\left(-\frac{\beta_{RD_2} d_{RD_2}^{\theta} (C_{T_2} - 1)}{\alpha_2 \rho_{RD_2}}\right) \\
\times \sum_{j=0}^{\mu_{RD_2}-1} \frac{(\beta_{RD_2} d_{RD_2}^{\theta})^j}{(\alpha_2 \rho_{RD_2})^j j!} \sum_{q=0}^{j} \binom{j}{q} (C_{T_2} - 1)^{j-q} \\
\times (C_{T_2}\alpha_2)^q \frac{\Gamma(\mu_{RE} + q)}{\left(\beta_{RD_2} d_{RD_2}^{\theta} \frac{C_{T_2}}{\rho_{RD_2}} + \frac{\beta_{RE} d_{RE}^{\theta}}{\rho_{RE}}\right)^{\mu_{RE}+q}}
\end{aligned} \tag{5.37}
$$

and

$$
\begin{aligned}
P_{SOP_2}^{\rho_{RD_2} \to \infty} = 1 - \Big(1 - \sum_{k=0}^{L_S} \binom{L_S}{k} (-1)^k \Phi \Psi_2 \frac{\beta_{SP}^{m_{SP}}}{\Gamma(m_{SP})} \\
\times (\Theta + m_{SP} - 1)! (k\beta_{SR}\gamma_{th_2} + \beta_{SP})^{-\Theta - m_{SP}}\Big) \\
\times \frac{(\beta_{RE} d_{RE}^{\theta})^{\mu_{RE}}}{\rho_{RE}^{\mu_{RE}} \Gamma(\mu_{RE})} \left(1 - \frac{\beta_{RD_2} d_{RD_2}^{\theta} (C_{T_2} - 1)}{\alpha_2 \rho_{RD_2}}\right) \\
\times \sum_{j=0}^{\mu_{RD_2}-1} \frac{(\beta_{RD_2} d_{RD_2}^{\theta})^j}{(\alpha_2 \rho_{RD_2})^j j!} \sum_{q=0}^{j} \binom{j}{q} (C_{T_2} - 1)^{j-q} \\
\times (C_{T_2}\alpha_2)^q \frac{\Gamma(\mu_{RE} + q)}{\left(\frac{\beta_{RE} d_{RE}^{\theta}}{\rho_{RE}}\right)^{\mu_{RE}+q}}.
\end{aligned} \tag{5.38}
$$

5.4 Performance Evaluation

5.4.1 Numerical Results and Discussions

In this section, we discuss the numerical and simulation results. The parameters are set as $\rho_I = 15\,\text{dB}$, $\rho_{RE} = 10\,\text{dB}$, $\alpha_1 = 0.85$, $\alpha_2 = 0.15$, $\theta = 2$, $K_{SR} = 80\,\text{m}$, $K_{RD_1} = 80\,\text{m}$, $K_{RD_2} = 60\,\text{m}$, $K_{RE} = 280\,\text{m}$, $H = 60\,\text{m}$, $m_{SP} = m_{SR} = m_{RD_1} = m_{RD_2} = m_{RE} = 2$, $\Omega_{SP} = \Omega_{SR} = \Omega_{RD_1} = \Omega_{RD_2} = \Omega_{RE} = 1$, $C_{th_1} = 0.0005$ bits/s/Hz, $C_{th_2} = 0.001$ bits/s/Hz, $N = 50$, and $L_S = L_{D_1} = L_{D_2} = L_E = 2$.

Figures 5.2 and 5.3 plot the impact of ρ_{RD_1} and ρ_{RD_2} on the SOP performance for D_1 and D_2 under different H, respectively. We can observe from those two figures that the secrecy performance is enhanced as ρ_{RD_1} (ρ_{RD_2}) increases due to the channel advantage of the legitimate link over the eavesdropping one. Furthermore,

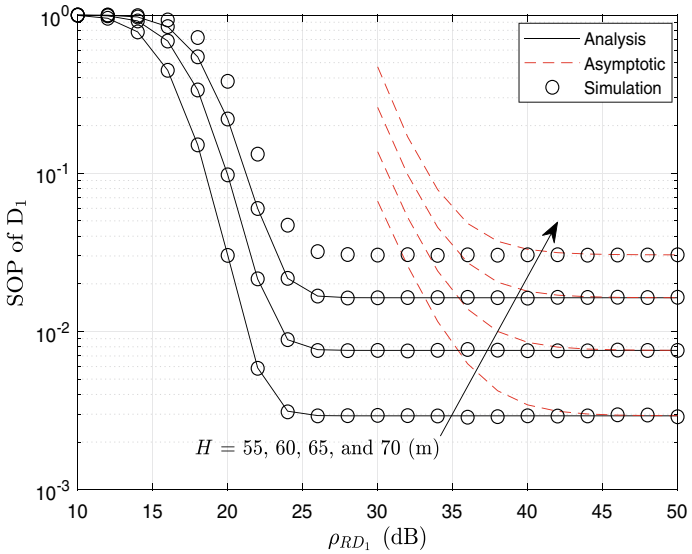

Fig. 5.2 SOP of D_1 versus ρ_{RD_1} for various H

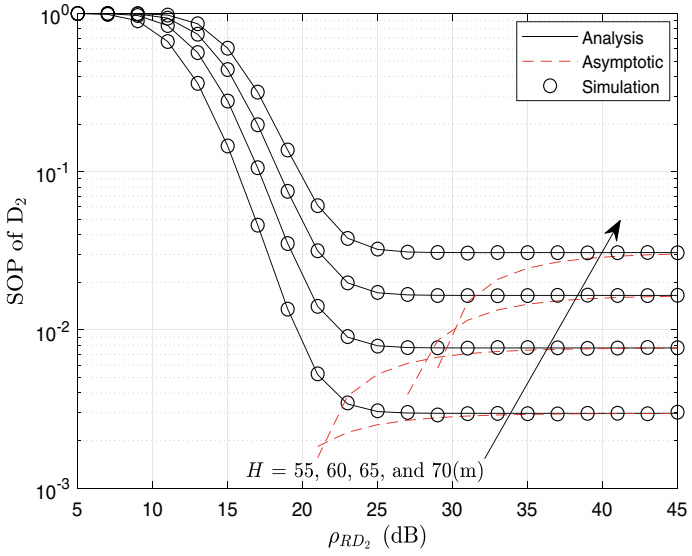

Fig. 5.3 SOP of D_2 versus ρ_{RD_2} for various H

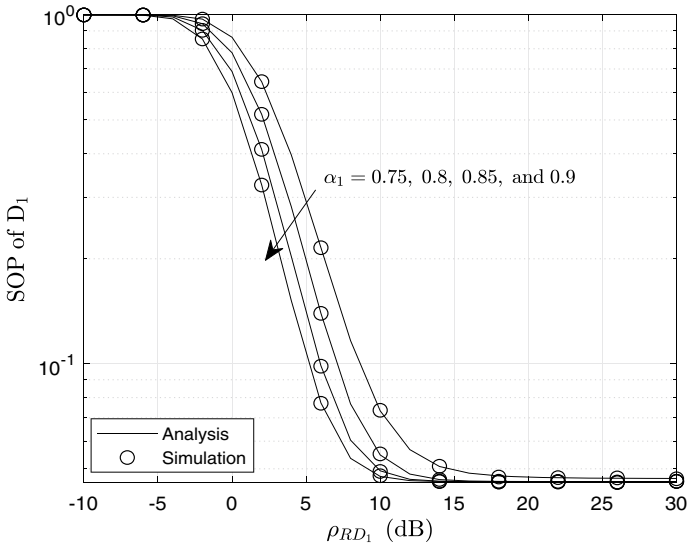

Fig. 5.4 SOP of D_1 versus ρ_{RD_1} for various α_1

the asymptotic results are approximate with the exact ones at the high SNR regions. However, it is also observed that when ρ_{RD_1} and ρ_{RD_2} are in the comparably high SNR region, i.e., $\rho_{RD_1} > 28\,\text{dB}$ in Fig. 5.2 and $\rho_{RD_2} > 24\,\text{dB}$ in Fig. 5.3, the SOP performance almost remains unchanged with ρ_{RD_1} (ρ_{RD_2}) increases. This is because the worst hop dominates the performance in the dual-hop link. In addition, one can see that a larger value of H corresponds to a worse SOP performance as a higher path loss resulted.

The SOP performance versus ρ_{RD_1} and ρ_{RD_2} for varying α_1 and α_2 are presented in Figs. 5.4 and 5.5. One can observe that the SOP performance enhances as $\alpha_1(\alpha_2)$ increases. A higher $\alpha_1(\alpha_2)$ means more power is allocated to the corresponding user.

The SOP versus ρ_I for D_1 and D_2 under various ρ_{RD_1} and ρ_{RD_2} are depicted in Figs. 5.6 and 5.7. We can see that the SOP performance enhances with the increase of ρ_I, as more power can be used for information transmission at S. Furthermore, as expected, the asymptotic results are approximate with the exact ones at the high SNR regimes.

Figures 5.8 and 5.9 plot the SOP versus ρ_{RE} for varying ρ_{RD_1} and ρ_{RD_2}. One can reveal that the SOP performance improves as the ρ_{RE} value decreases. This is because a smaller value of ρ_{RE} means a poorer natural communication environment for the eavesdropper.

The impact of the number of antennas on the SOP performance is illustrated in Figs. 5.10 and 5.11. One can see that the value of SOP decreases as L_{D_i} increases when $\rho_{RD_1} < 24\,\text{dB}$ in Fig. 5.10 and $\rho_{RD_2} < 36\,\text{dB}$ in Fig. 5.11. This is because a higher diversity gain can be obtained when more antennas are available on the device. When ρ_{RD_i} exceeds a certain value, i.e., $\rho_{RD_1} > 24\,\text{dB}$ and $\rho_{RD_2} > 36\,\text{dB}$, the secrecy

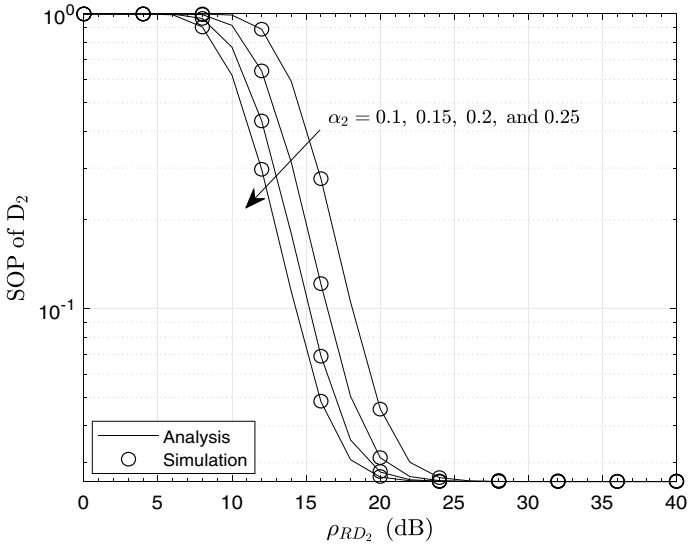

Fig. 5.5 SOP of D_2 versus ρ_{RD_2} for various α_2

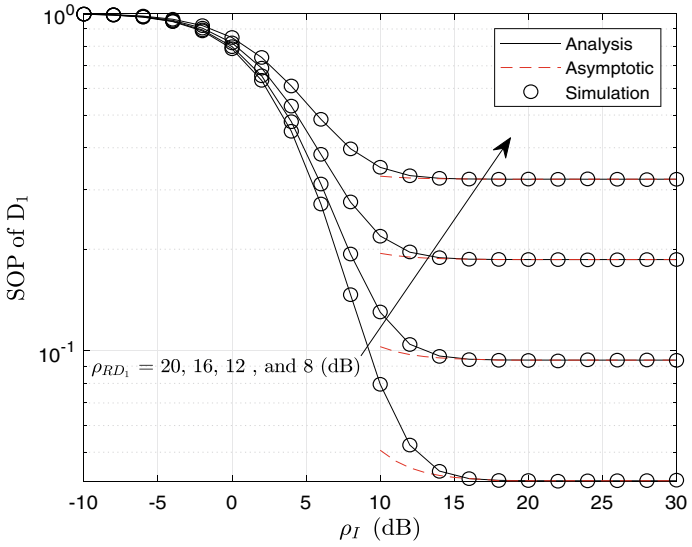

Fig. 5.6 SOP of D_1 versus ρ_I for various ρ_{RD_1}

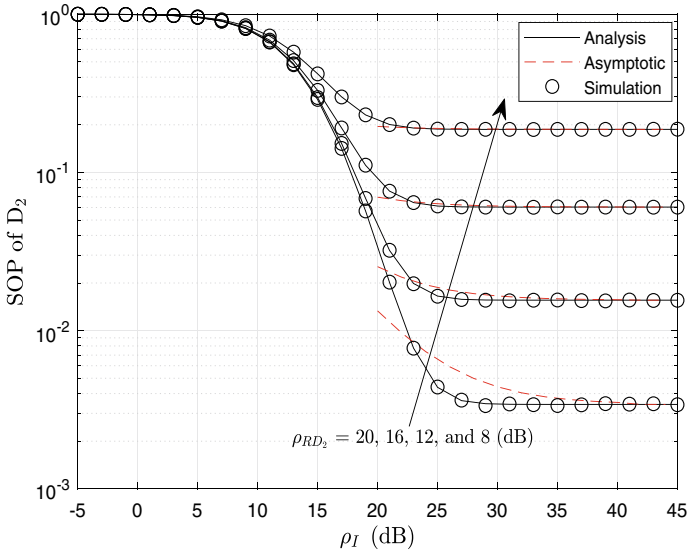

Fig. 5.7 SOP of D_2 versus ρ_I for various ρ_{RD_2}

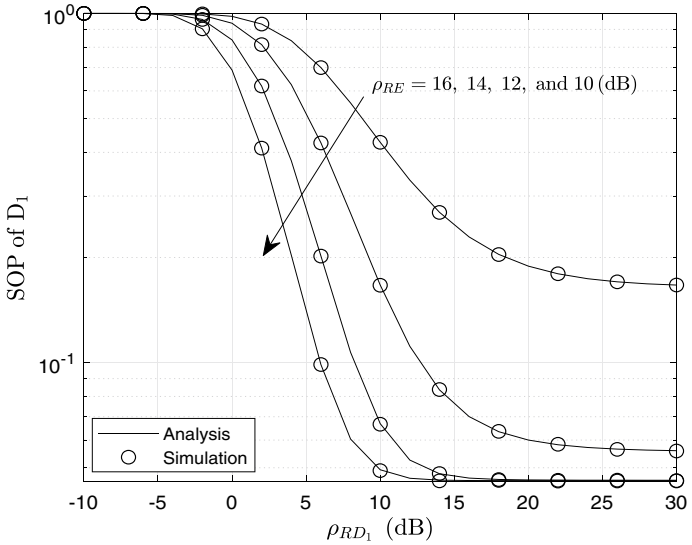

Fig. 5.8 SOP of D_1 versus ρ_{RD_1} for various ρ_{RE}

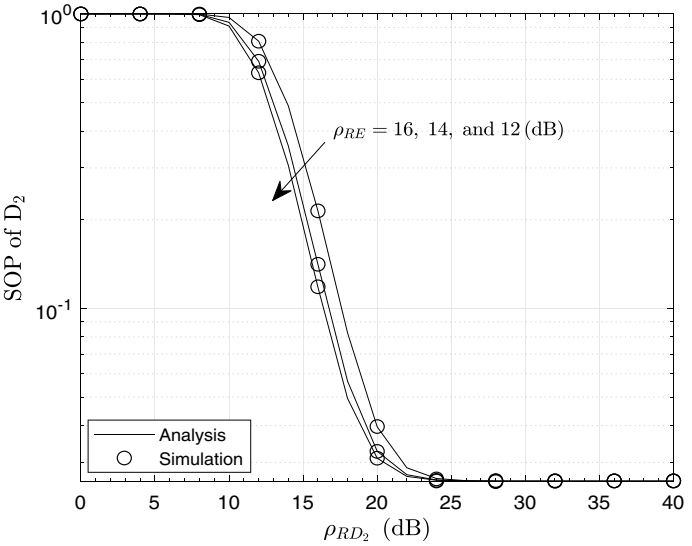

Fig. 5.9 SOP of D_2 versus ρ_{RD_2} for various ρ_{RE}

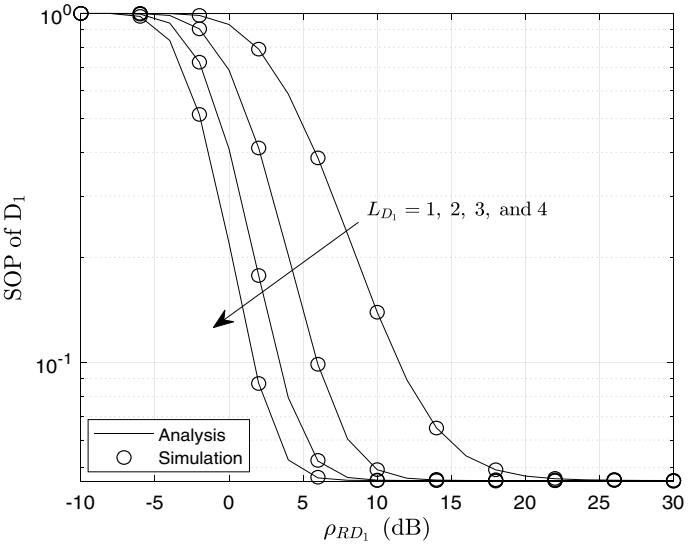

Fig. 5.10 SOP of D_1 versus ρ_{RD_1} for various L_{D_1}

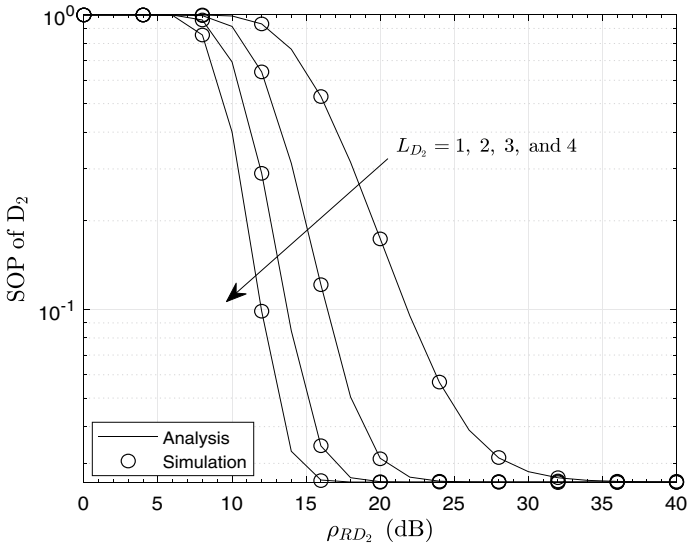

Fig. 5.11 SOP of D_2 versus ρ_{RD_2} for various L_{D_2}

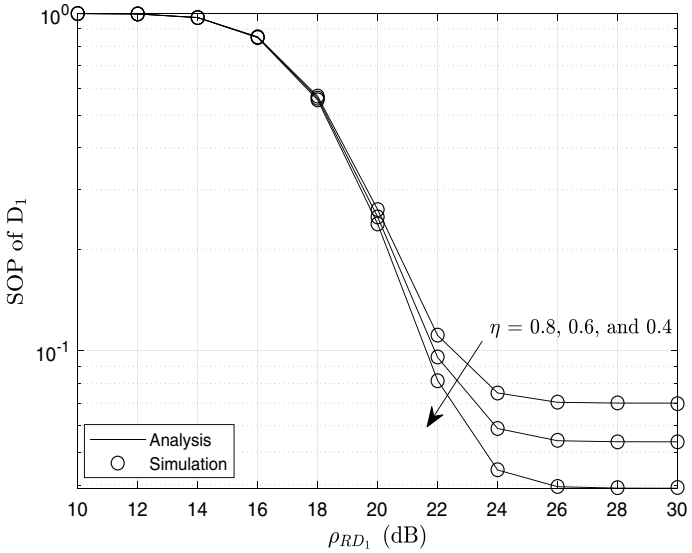

Fig. 5.12 SOP of D_1 versus ρ_{RD_1} for various η

performance is almost similar for the different number of antennas, which is because the first hop dominates the system performance.

The impact of scaling coefficient η on the SOP performance is presented in Figs. 5.12 and 5.13. As illustrated in those two figures, it is observed that the SOP

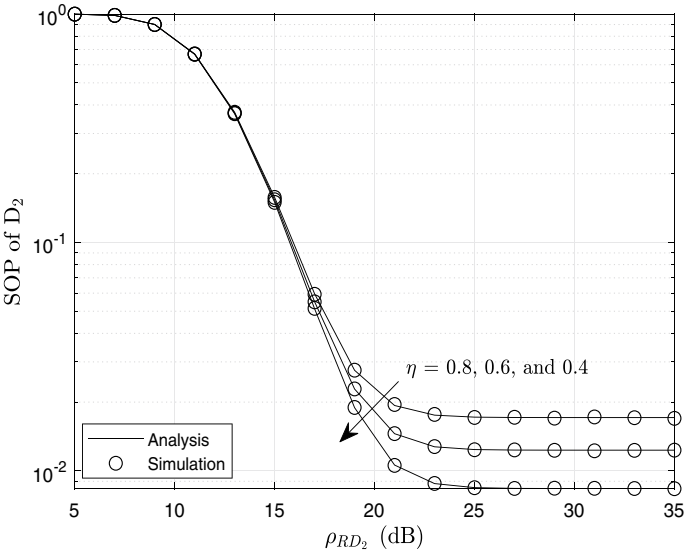

Fig. 5.13 SOP of D_2 versus ρ_{RD_2} for various η

performance improves as the value of η decreases. This is because a smaller value of η means less interference from the primary transmitter, which can result in better SOP performance.

5.4.2 SOP for the UAV with Different Spatial Positions and a Constant Speed

This section presents the SOP performance when the UAV has different spatial positions and flies at a constant speed. For convenience, as shown in Fig. 5.14, the positions of S, R, D_i, and E are presented in a three-dimensional coordinate, which are (x_S, y_S, z_S), (x_R, y_R, z_R), $(x_{D_i}, y_{D_i}, z_{D_i})$, and (x_E, y_E, z_E). Unless otherwise specified, the initial coordinates of those nodes are set as S (0, 0, 0), R (30, 30, 60), D_1 (90, 90, 0), D_2 (70, 70, 0), and E (230, 230, 0), and the unit is meter (m).

Scenario 1: UAV is with different spatial positions.
In this scenario, the distance between the UAV and the node g ($g \in \{S, D_1, D_2, E\}$) can be re-expressed using the three-dimensional coordinates as

$$d_{Rg} = \sqrt{(x_R - x_g)^2 + (y_R - y_g)^2 + (z_R - z_g)^2}. \tag{5.39}$$

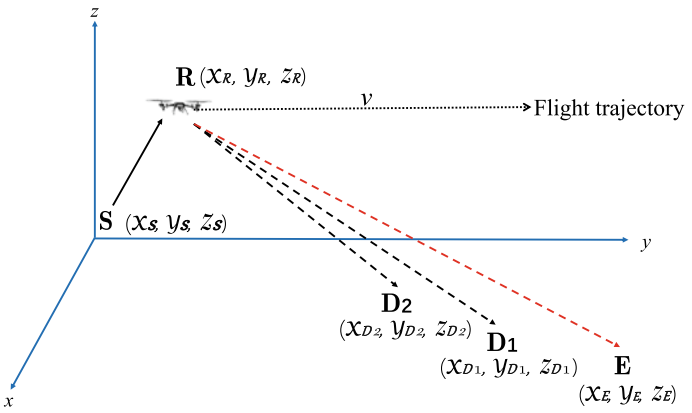

Fig. 5.14 Three-dimensional coordinate model and the flight trajectory of the UAV with a constant speed

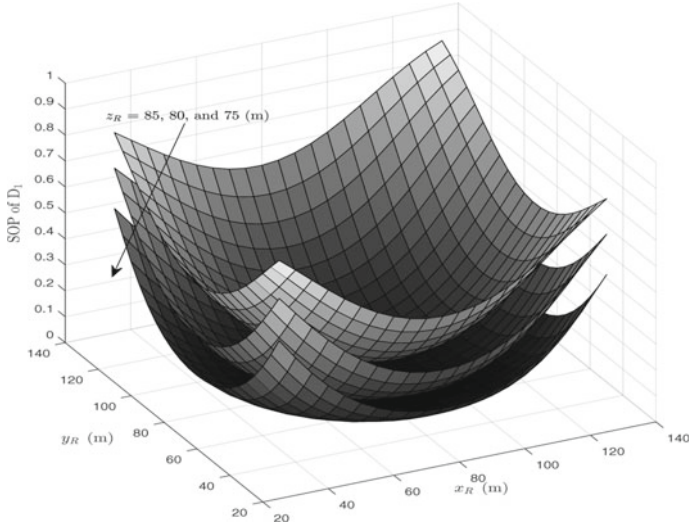

Fig. 5.15 SOP of D_1 versus the UAV deployment position under various z_R with $\alpha_1 = 0.8$

The results are presented in Figs. 5.15 and 5.16. Those two figures show that an optimal UAV deployment position exists for each curve in which the secrecy outage performance is the best.

Scenario 2: UAV flies with a constant speed.
As shown in Fig. 5.14, a simple scenario in which the UAV flies horizontally along with the y-axis to the right with a constant speed v is considered. Therefore, the distance between the UAV and the node g is

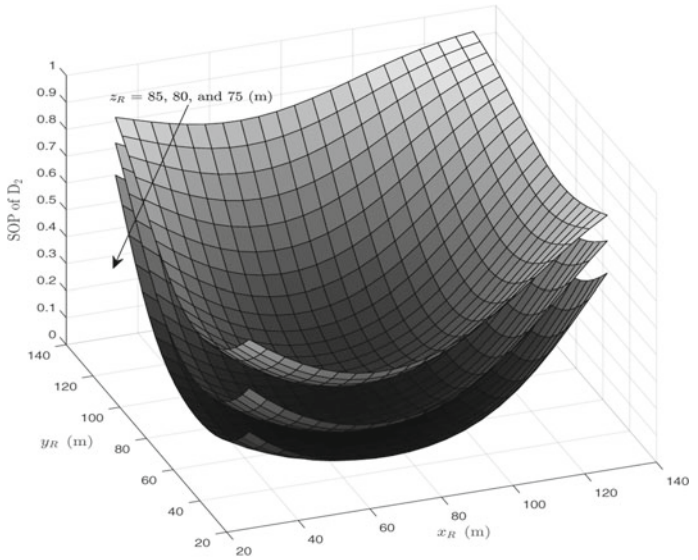

Fig. 5.16 SOP of D_2 versus the UAV deployment position under various z_R with $\alpha_1 = 0.8$

$$d_{Rg} = \sqrt{(x_R - x_g)^2 + (y_R + vt - y_g)^2 + (z_R - z_g)^2}, \tag{5.40}$$

where t is the flight time. As illustrated in Fig. 5.17, one can observe that the SOP performance for both users first improves and then decreases as the UAV flies. This is because the UAV first approaches and then flies away from the users, which decreases the distance between the UAV and the users and increases.

From the above two scenarios, we can conclude that it is better to allocate the UAV in a proper position to result in the best secrecy performance of the system.

Last but not least, compared with previous works on multi-antenna scenarios for UAV-NOMA systems, it is noted that the purpose of adopting multi-antenna is to cover different sectors [11], or to realize the beamforming [12–14], or to employ directional modulation [15]. Unlike those previous works, our focus of employing multi-antenna in this study is on diversity-combining techniques regarding SOP performance, i.e., both TAS at the source and MRC at the destinations. The primary technical challenge of the analysis includes but is not limited to obtaining the PDF and CDF expressions for the TAS output in the presence of underlay cognitive radio and the MRC output, as well as doing the asymptotic analysis. Numerical results from the analytical and asymptotic expressions show that the asymptotic results approximate the exact ones at the high SNR regions. Furthermore, it is also found that those figures have an error floor because another hop with fixed SNRs dominates the system performance.

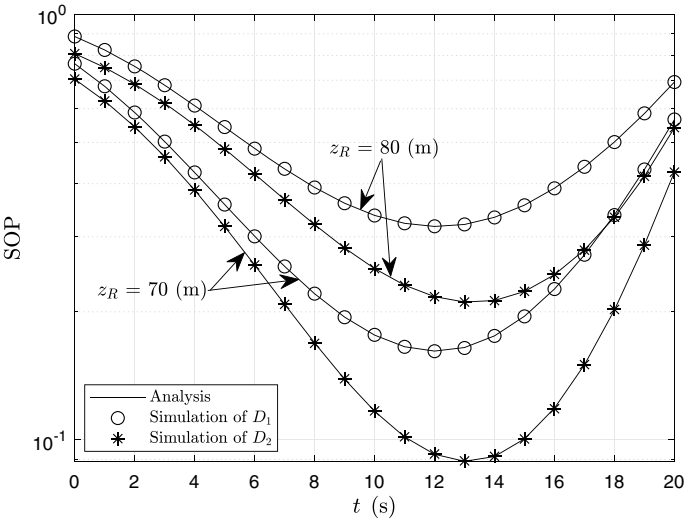

Fig. 5.17 SOP versus the trajectory of the UAV with D_1 (90, 70, 0), and $v = 5$ m/s

5.5 Conclusion

This section analyzes the secrecy performance for an underlay CR-based UAV-aided NOMA system over Nakagami-*m* fading channels. Both users' analytical and asymptotic expressions of SOP have been obtained when the TAS scheme is adopted at a secondary source and the MRC protocol is deployed at the destinations. Furthermore, we have analyzed the effects of the number of antennas, power distribution coefficient, height of the UAV, and interference power threshold on the secrecy performance. Numerical results illustrate that increasing the average SNR can enhance the secrecy performance, and the worse hop dominates the secrecy performance of the whole link. Moreover, increasing the number of receiving antennas, interference power threshold, and power distribution coefficient can also enhance the SOP performance of the system. In contrast, the system performance deteriorates as the height of the UAV increases. In addition, an optimal UAV deployment position makes the secrecy outage performance the best.

References

1. Y. Zeng, R. Zhang, T.J. Lim, Wireless communications with unmanned aerial vehicles: opportunities and challenges. IEEE Commun. Mag. **54**(5), 36–42 (2016)
2. L. Gupta, R. Jain, G. Vaszkun, Survey of important issues in UAV communication networks. IEEE Commun. Surv. Tuts. **18**(2), 1123–1152 (2016)

3. A.A. Khuwaja, Y. Chen, N. Zhao, M.-S. Alouini, P. Dobbins, A survey of channel modeling for UAV communications. IEEE Commun. Surv. Tuts. **20**(4), 2804–2821 (2018)
4. X. Cai et al., *Low Altitude UAV Propagation Channel Modelling*, in 2017 11th European Conference on Antennas and Propagation (EUCAP) (2017), pp. 1443–1447
5. W. Khawaja, I. Guvenc, D. Matolak, *UWB Channel Sounding and Modeling for UAV Air-to-ground Propagation Channels*, in 2016 IEEE Global Communications Conference (GLOBECOM) (2016), pp. 1–7
6. I.S. Gradshteyn, I.M. Ryzhik, *Table of Integrals, Series, and Products*, 7th edn. (Academic press, San Diego, 2007)
7. S. Arzykulov, G. Nauryzbayev, T.A. Tsiftsis, B. Maham, Performance analysis of underlay cognitive radio nonorthogonal multiple access networks. IEEE Trans. Veh. Technol. **68**(9), 9318–9322 (2019)
8. D.-T. Do, A.-T. Le, B.M. Lee, NOMA in cooperative underlay cognitive radio networks under imperfect SIC. IEEE Access **8**, 86180–86195 (2020)
9. W. Han, J. Ge, J. Men, Performance analysis for NOMA energy harvesting relaying networks with transmit antenna selection and maximal-ratio combining over Nakagami-*m* fading. IET Commun. **10**(18), 2687–2693 (2016)
10. Z. Wei, D.W.K. Ng, J. Yuan, Joint pilot and payload power control for uplink MIMO-NOMA with MRC-SIC receivers. IEEE Commun. Lett. **22**(4), 692–695 (2018)
11. T.M. Nguyen, W. Ajib, C. Assi, A novel cooperative NOMA for designing UAV-assisted wireless backhaul networks. IEEE J. Sel. Areas Commun. **36**(11), 2497–2507 (2018)
12. T. Hou, Y. Liu, Z. Song, X. Sun, Y. Chen, Multiple antenna aided NOMA in UAV networks: a stochastic geometry approach. IEEE Trans. Commun. **67**(2), 1031–1044 (2019)
13. N. Rupasinghe, Y. Yapici, I. Guvenc, Y. Kakishima, Non-orthogonal multiple access for mmWave drone networks with limited feedback. IEEE Trans. Commun. **67**(1), 762–777 (2019)
14. Y. Yapici, N. Rupasinghe, I. Guvenc, H. Dai, A. Bhuyan, Physical layer security for NOMA transmission in mmWave drone networks. IEEE Trans. Veh. Technol. **70**(4), 3568–3582 (2021)
15. X. Sun, W. Yang, Y. Cai, Secure communication in NOMA-assisted millimeter-wave SWIPT UAV networks. IEEE Internet Things J. **7**(3), 1884–1897 (2020)